Journal of the European Ceramic Society 22 (2002) 745–754

www.elsevier.com/locate/jeurceramsoc

Mechanical properties of magnesia-spinel composites

Cemail Aksel[1], Brian Rand, Frank L. Riley*, Paul D. Warren[2]

Department of Materials, School of Process, Environmental and Materials Engineering, University of Leeds, Leeds LS2 9JT, UK

Received 10 February 2001; received in revised form 17 May 2001; accepted 21 May 2001

Abstract

A set of dense magnesia-magnesium aluminate spinel composites has been prepared by hot-pressing magnesia powder using 0 to 30 wt.% of spinel powder of mean particle size 3, 11 and 22 μm. Bend stength, modulus, and fracture toughness, have been measured. Strength and modulus decrease with increasing spinel content, and for a given loading, spinel particle size, as a result of microcracking caused by thermal expansion mismatch between the magnesia matrix grains and the spinel particles, the effects of which may be intensified by recrystallization of spinel. Fracture is predominantly transgranular for the pure magnesia, and intergranular for the composite materials. Possible reasons for the differences in behaviour between this system and the SiC–Al_2O_3 system with a similar thermal expansion mismatch are examined.

Keywords: Fracture toughness; Magnesite refractories; $MgAl_2O_4$; MgO; Modulus; Refractories; Residual stress; Spinel; strength; Thermal expansion

1. Introduction

Magnesite–chrome and chrome–magnesite refractories have been used over many years as high strength hot-face refractories in a wide range of furnaces. They have important applications where a very high degree of refractoriness or resistance to basic environments is required, such as steel making vessels and rotary cement kilns.[1] These refractories are produced by blending crushed magnesite and chrome ore. Chrome ore is a mixture of spinels of the general stoichiometry $R(II)R[III]_2O_4$, where a significant proportion of the trivalent cation R[III] is Cr^{3+}. However, because of the risk of contamination of ground water by Cr[VI] ions leached from waste refractory materials, and because Cr[VI] has in particular been associated with allergic skin ulceration and carcinomas, the replacement of the chrome in these refractories is considered to be very desirable.[2–4] For this reason attention has been given to the use of magnesium aluminate spinel, $MgAl_2O_4$, as an alternative to chrome ore.[5–7] While magnesite is often used alone, magnesium aluminate spinel is now widely incorporated in magnesite-based refractories:[8,9] an example of their use is in the cooling zone and the upper side of the sintering zone of cement kilns. A further major advantage of the magnesite-spinel refractories is that they have improved thermal shock resistance, and it is claimed that two to three times longer service life can be obtained, compared to a conventional magnesite-chrome brick.[4,10,11] The reason for the improved thermal shock resistance has been linked to the large difference in thermal expansion coefficient between magnesia ($\sim$13.5 MK^{-1}) and $MgAl_2O_4$ ($\sim$7.6 MK^{-1}).[12–14] It is believed that on cooling from fabrication temperatures in the region of 1700 °C, the thermal expansion mismatch leads to large tensile hoop stresses and microcrack development around the spinel grains. Because commercial refractories always contain silicates some transient healing of the cracks may occur on subsequent reheating during use, but the importance of microcracking for mechanical properties is not in doubt.[10,15,16] What have not been investigated, however, are the factors controlling the extent of microcrack generation in the magnesia-spinel system, to provide a basis of understanding of the behaviour of these composite materials, so that optimum compositions can be identified. In practice the materials' requirements are largely established by trial and error.[17,18]

We report here a study of the effects of the presence of magnesium aluminate (spinel) particles in high purity

* Corresponding author.
E-mail address: f.l.riley@leeds.ac.uk (F.L. Riley).
[1] Now at: Department of Ceramic Engineering, Anadolu University, İki Eylül Kampüsü, 26470 Eskişehir, Turkey.
[2] Now at: Pilkington plc., Group Research, Technology Centre, Hall Lane, Lathom, Lancs. L40 5UF, UK.

0955-2219/02/$ - see front matter
PII: S0955-2219(01)00373-9

and fully dense and relatively fine grain magnesia. This system was chosen partly as a simplified laboratory model for commercial refractory materials, which contain a range of magnesite particle sizes, including very coarse (to cm size) grains. However, in these refractories a finer particle fraction of material is commonly used to bond the much coarser magnesite grains, and the overall mechanical properties and service behaviour of the refractory are likely to be strongly influenced by the bond phase. There is additional merit therefore in studying systems corresponding to this bond phase. The intention of this work was to establish the separate influences of spinel particle size and level of addition, on the mechanical properties, and the basis for the observed thermal shock behaviour, of these model finer grain composite materials. This paper reports measurements of those mechanical property values needed for the calculation of the Hasselman thermal shock (R) parameters.[19]

2. Experimental

The starting high purity magnesium oxide (Light: GPR, BDH., Poole UK; $\geqslant$98% MgO) was a nanoparticle size ($\sim$30 nm) powder. To improve densification behaviour it was necessary to carry out a preliminary calcination at 1300 °C for 2 h, which yielded a powder of apparent mean particle size $\sim$0.5 μm. The spinel powder was a commercial material (MR66 grade, Alcoa, UK) of 99.5% purity, which was milled and then air-classified (Alpine Zig-zag classifier, Augsburg, Germany) to produce three fractions of narrow size range with medians of $\sim$3, $\sim$11 and $\sim$22 μm. Stated impurities are given in Table 1. Particle sizes were measured by a standard laser scattering method (Mastersizer, Malvern Instruments, Malvern UK).

MgO-spinel mixtures with 5, 10, 20 or 30% by weight of spinel were prepared, together with pure MgO reference material. Powders were blended by milling in isopropanol, followed by drying at 110 °C and passing through a 100 μm sieve to break up large agglomerates. Densification was achieved by hot-pressing in a graphite die with a pressure of 20 MPa for 20 min, at temperatures between 1650 and 1725 °C. Discs of 30 mm diameter and 5 mm thickness were produced, of density > 99% of theoretical, calculated assuming densities of 3.59 Mg m^{-3} for MgO, and of 3.58 Mg m^{-3} for spinel[a] Bulk density was measured using the standard water immersion method (BS7134).[20] To obtain suitable samples for mechanical property measurements, disc surfaces were ground with progressively finer SiC grits down to 1000 mesh, and the tensile faces were finally diamond polished to 1 μm. Discs were then cut into bars $\sim$26×3×3 mm^3 for strength, and single edge notched beam (SENB) fracture toughness measurements. The long edges of the bars were uniformly chamfered at 45° to a depth of $\sim$0.2 mm, and rounded to a radius of $\sim$3 mm. Machining was carried out in a direction parallel to the long axis of the bar.[21]

Bend strength [21] was measured in three point loading with support roller span (L) of 20 mm, and a loading rate of 0.2 mm min^{-1}. Young's modulus (E) was calculated on the basis of the initial, steepest straight-line portion of the load-deflection curve, with correction for machine stiffness,[22] using the standard relationship:

$$E = L^3 m/\left(4wd^3\right) \tag{1}$$

where m is the initial slope of the curve, w is the bar width, and d the bar thickness. The mean values given were obtained on the basis of five measurements. Fracture toughness specimens were cut in the centre of the bar with a 50 μm diamond blade to a depth (c) of 0.75 mm, to give a notch depth to thickness ratio of 0.25. K_{1c} values were calculated from the fracture load (P) using the standard equation:[23–26]

$$K_{1c} = \left\{3PLc^{1/2}.Y\right\}/\left\{2wd^3\right\} \tag{2}$$

where Y is given by:

$$Y = A_0 + A_1(c/d) + A_2(c/d)^2 + A_3(c/d)^3 + A_4(c/d)^4 \tag{3}$$

For $L/d \sim 8$, $A_0 = 1.96$, $A_1 = -2.75$, $A_2 = 13.66$, $A_3 = -23.98$, $A_4 = 25.22$.[25]

Materials were polished to 1 μm diamond and thermally etched at 1500 °C for 10 min to reveal grain boundaries in the scanning electron microscope (Cambridge Instruments CamScan 4). Mean grain sizes were calculated using the standard mean intercept method [27] from several hundred grains in three photographs for each sample. Secondary electron images were used to examine the size and shape of grains exposed in fracture surfaces; back scattered images were used to identify the presence and position of spinel particles.

Table 1
Starting powder purity (% by weight)

MgO	As ion	Fe^{3+}	$C1^-$	SO_4^{2-}			
		0.05	0.15	0.5			
Spinel	As oxide	CaO	Fe_2O_3	Na_2O	TiO_2	MnO	P_2O_5
		0.2	0.1	0.01	0.01	0.01	0.01

[a] ICDD set 47, files 45-946 and 21-1152.

3. Results

All materials were practically fully dense and porosity was not considered likely to be a factor controlling strength, as would be expected for higher levels of porosity and as has been reported in previous studies on hot-pressed MgO.[28] The mean grain size for pure MgO produced by hot-pressing at 20 MPa for 25 min at 1650 °C was 30 μm, and the strength of 250 MPa was consistent with earlier measurements on material of similar grain size.[28–30] The MgO grain size of the composite was controlled by spinel loading, and particle size. There was a marked increase for spinel additions of 5–10%, but higher spinel additions led to a decrease in size, with a trend towards values close to those of pure MgO, as shown in Fig. 1. Composite bend strength decreased uniformly with increasing additions of spinel, and with increasing spinel particle size, as shown in Fig. 2. Strength as a function of particle size for constant spinel loading (illustrated by 10% addition) is shown in Fig. 3. The Young's modulus showed a similar general trend to that of strength (Fig. 4) and decreased with increasing spinel content and particle size. The maximum value for pure MgO was 268 GPa, in reasonable agreement with previously reported values of 290 GPa [28] and 258 GPa.[31]

Fracture toughness values are shown in Fig. 5. The measured value of 2.2 MPa $m^{1/2}$ for the pure MgO (mean grain size ~32 μm) is in good agreement with a literature value of ~2.05 MPa $m^{1/2}$ for materials of grain size 6–8 μm.[32] Toughness decreased by ~50% with additions up to 10%, and values then remained constant within experimental error. Fracture surface energy values obtained from modulus and SENB toughness values using the standard relationship:

$$\gamma_i = K_{Ic}^2/2E \quad (4)$$

are shown in Fig. 6. The calculated value of γ_i for the pure MgO (grain size 30 μm) was in the region of 9 J m^2. Previous reported values are 14 J m^{-2} for MgO of grain size ~100 μm[33–35] and 15 J m^{-2}.[34] Values of γ_i have

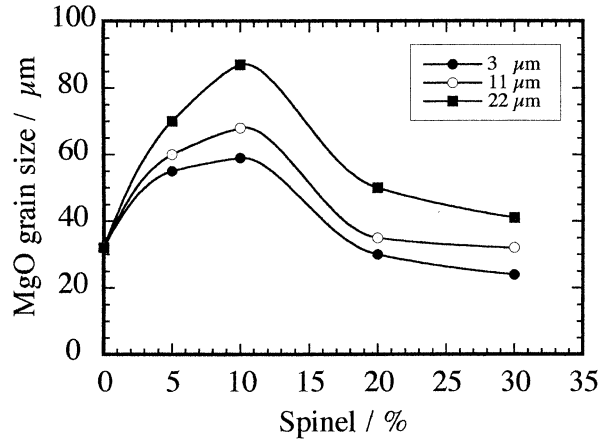

Fig. 1. MgO mean grain size as a function of spinel content and mean particle size.

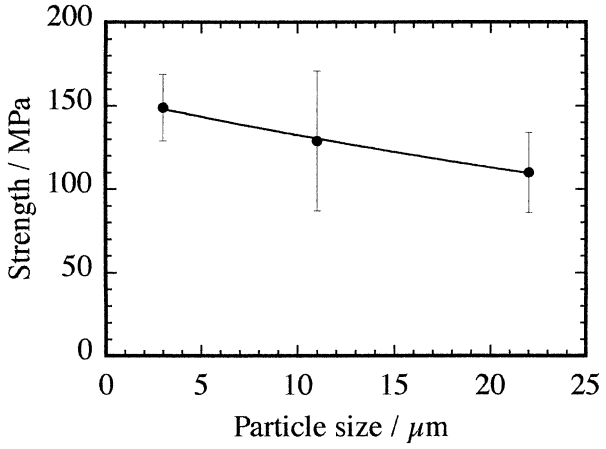

Fig. 3. Strength as a function of particle size at 10% spinel loading.

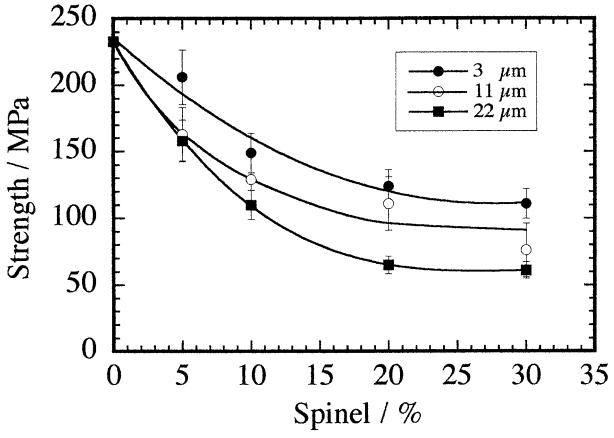

Fig. 2. Strength as a function of spinel content and mean particle size.

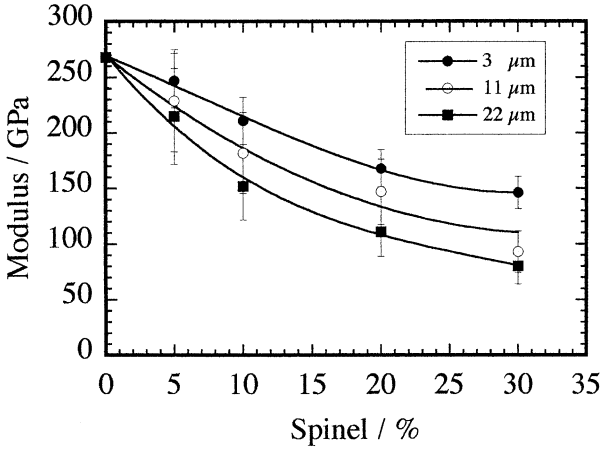

Fig. 4. Young's Modulus as a function of spinel content and mean particle size.

also been reported for dense spinel; these are lower, and in the range 4–7 J m^{-2}.[36–38] Combining the SENB fracture toughness values with those of strength allowed an estimate to be made of the critical defect size. Values are shown in Fig. 7. For pure MgO the critical defect size was of the order of 28 μm, close to the measured mean grain size. The effect of spinel loading was not great: with 5–10% additions of spinel the critical defect size was unchanged or smaller than the measured MgO grain size. With increased additions the defect size rose steadily, reaching 40–50 μm at 30% addition.

Fracture faces of pure MgO show pronounced transgranular fracture, with clear grain facetting. A typical face is shown in Fig. 8. The composites showed a marked tendency towards intergranular fracture, the tendency being more marked the higher the spinel loading, as illustrated by Fig. 9(a) for 5%, and 9(b) for 30% additions of 22 μm spinel.

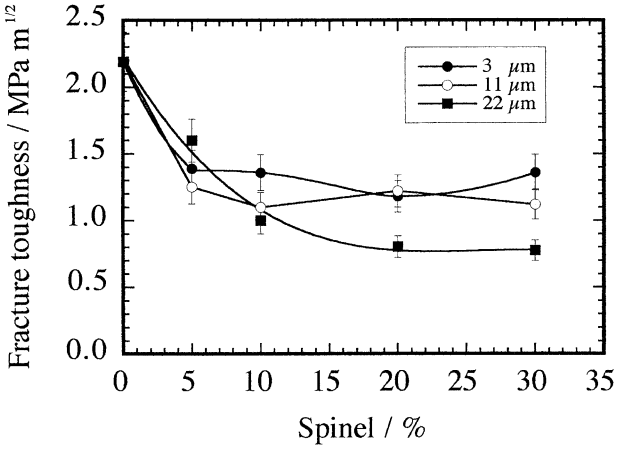

Fig. 5. Fracture toughness as a function of spinel content and mean particle size.

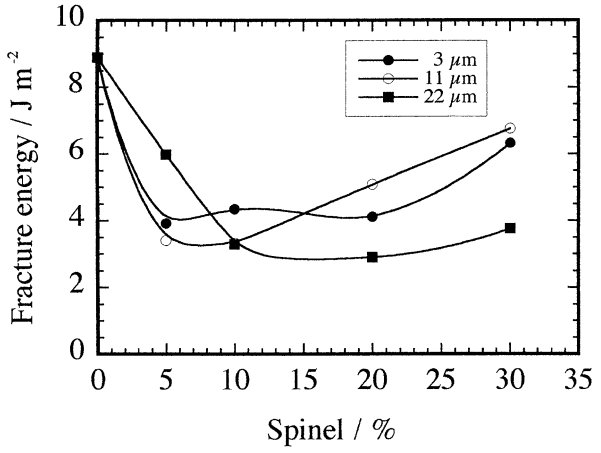

Fig. 6. Fracture surface energy as a function of spinel content and mean particle size.

4. Discussion

The spinel is not a completely inert component of this system, as is shown by the marked changes occurring in the grain size of the MgO matrix. There appear to be two influences of the spinel particles. Small additions clearly accelerate grain growth, probably by increasing point defect mobility as a result of extensive doping of the MgO crystal lattice with the aliovalent Al^{3+}. Al_2O_3 has appreciable solubility in MgO at high temperature, and it would be expected that the initial MgO-spinel system will attempt to form the equilibrium MgO(solid-solution)-spinel system. Data compiled by Henrikson and Kingery[39] (and subsequently reproduced by Hallstedt[40] by computer calculation) show that at the temperature

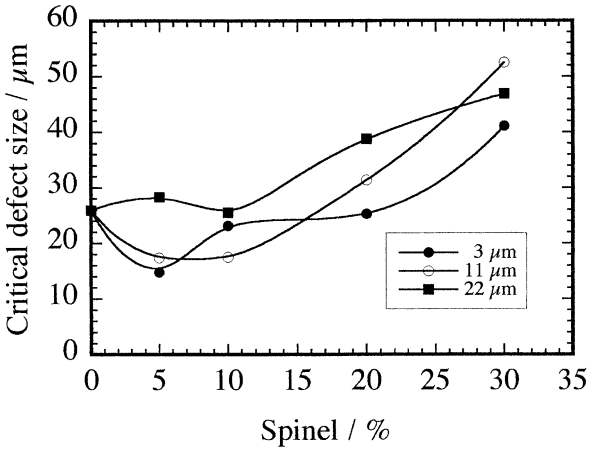

Fig. 7. Critical defect size as a function of spinel content and mean particle size.

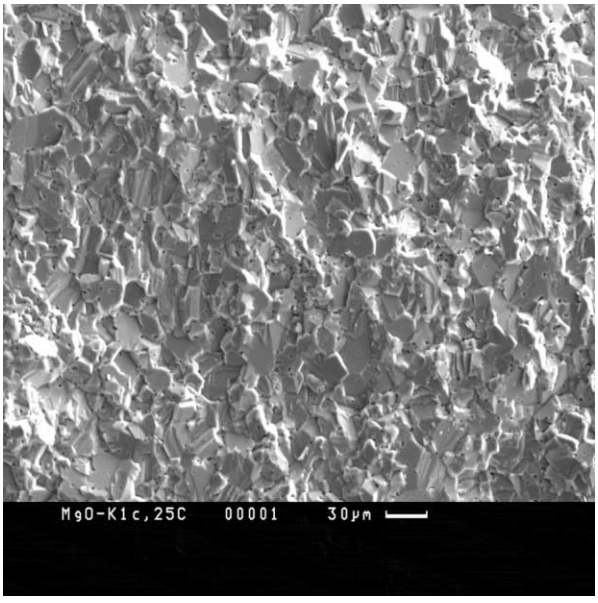

Fig. 8. SEM photograph of a fracture face of pure MgO, showing pronounced transgranular fracture.

of 1725 °C used for preparation of the composites, the equilibrium mole fraction of Al_2O_3 in solid solution in the MgO is about 0.018. This corresponds to an MgO solid solution containing 4.43% by weight of Al_2O_3, which is equivalent to about 6 wt.% of spinel (because of the closely similar densities of MgO and $MgAl_2O_4$ these values also closely reflect the amounts expressed as volumes). The spinel particles release Al_2O_3 and themselves partially or entirely convert to the MgO (solid solution) during densification. This effect is seen most strikingly in the composites prepared with only 5% spinel, and in which most of the larger spinel particles have disappeared, to be replaced by clusters of very small spinel particles precipitated at the MgO grain boundaries. It is of interest that in the relatively short time at maximum temperature even the largest (22 μm) spinel particles can interact, and only a small proportion of the original spinel is able to reform at the grain boundaries as the Al_2O_3 is exsolved during cooling. A typical microstructure for materials formed with 5% spinel, very similar to that presented by Henrikson and Kingery, is shown in Fig. 10 for 11 μm spinel. With increased additions (10% and upwards) of spinel, high temperature saturation of the MgO is achieved, and there are now significant proportions of spinel particles approaching the expected sizes in the microstructure, almost all located at the

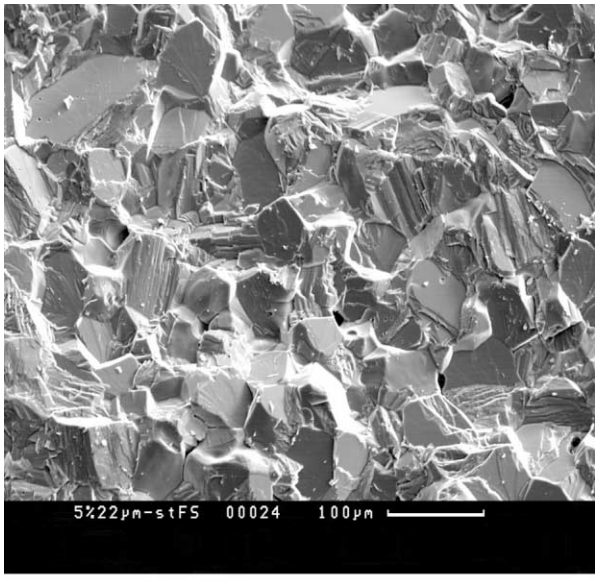

(a)

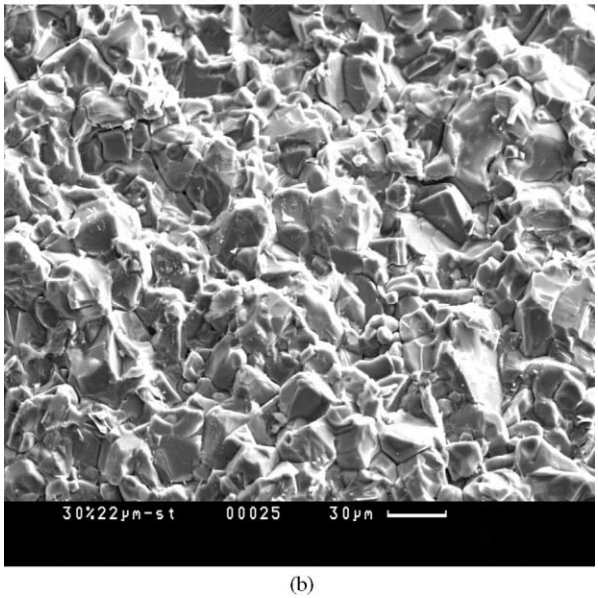

(b)

Fig. 9. SEM photograph of a fracture face of (a) 5% 22 μm spinel (b) 20% 22 μm spinel composites, showing predominantly intergranular fracture.

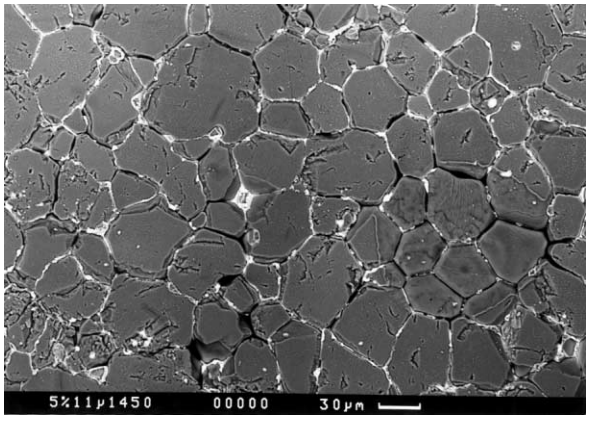

Fig. 10. SEM photograph of a 5% 11 μm spinel composite, showing the absence of the expected large particles, and the recrystallization of very fine spinel particles at grain boundaries.

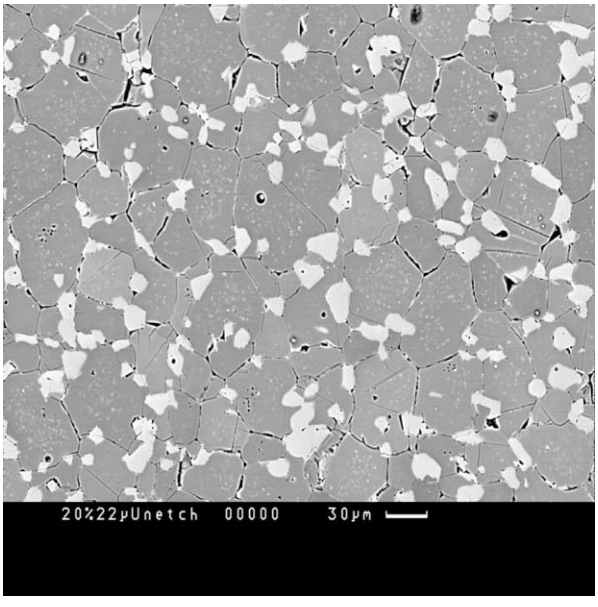

Fig. 11. SEM photograph of the polished surface of a 20% 22 μm spinel composite, showing the distribution of larger spinel particles at MgO grain boundaries, the fine intragranular spinel, and cracked MgO grains.

MgO grain boundaries, as shown in Fig. 11. This also shows the absence of fine spinel precipitates at the grain boundaries, suggesting that most of the precipitated spinel has grown on existing large particles. The spinel particles still tend to cluster at the MgO boundaries, with many direct spinel–spinel grain boundaries. From the detailed microstructural point of view these composites are thus not entirely homogeneous with respect to spinel particle location and distribution. The clustering and partial bonding of the spinel particles at the MgO boundaries also tends to blur somewhat the size distribution expected.

Because of the solubility of Al_2O_3 in MgO and incomplete re-equilibration on cooling (as indicated by the 5% composites) the actual spinel content of the composites is only approximately that of the amount added, and possibly 4–5% less. However, in this discussion the nominal (added) spinel amounts are used. Most of the spinel is located at the MgO–MgO grain boundaries (intergranular), but a small amount is present as very fine crystallites within the MgO grains (intragranular). The composites can thus be regarded as a duplex structures.

A second action of the spinel particles, more effective at higher loadings, appears to be that of reducing MgO grain boundary mobility through grain boundary pinning. The overall grain size-spinel content curve of Fig. 2 is thus likely to be a composite, created by the superposition of two opposing effects, with grain boundary velocity reaching a peak with saturation of the MgO by Al_2O_3 at about 6% spinel addition.

It is clear from Fig. 1 that the loss of strength in the composites is not the result of the influence of spinel on magnesia grain size. It is also clear that the spinel particles are not acting as simple critical defects, because for all materials the spinel particle size was much smaller than the magnesia grain size, which must be presumed to be the major critical defect dimension in the pure material, and for which smooth strength-grain size relationships have been seen [30]. The observed changes in composite strength with increasing spinel loading and particle size are consistent with the generation of microcracks. Direct evidence of microcracking is seen in polished faces, typified by Fig. 11. These microcracks, it has been assumed, are the result of the large thermal expansion mismatch between the MgO matrix grains and the spinel particles. In fact in very many cases, the intergranular cracking might be more accurately described as grain boundary separation. The microcracking becomes more extensive, the higher the spinel content. Much of the cracking appears to be intergranular, but with the more extensively cracked materials, cracks clearly also extend through MgO grains, following the natural cleavage planes. The decrease in strength of the spinel composites is, therefore, more likely to be related to a decrease of fracture toughness with decreasing E and fracture energy, and in particular to the change in nature of the critical defect from a more or less equiaxed MgO grain to a sharp planar grain boundary crack.

To facilitate analysis of the influence of the spinel particle on mechanical properties it is useful to have an idea of the spinel particle distribution, expressed in terms of the mean spinel-spinel separation distance. An estimate of this distance can be made by assuming some regular array of spherical particles dispersed in the MgO matrix. Using a simple cubic array of particles of diameter D and volume fraction V_p, the mean interparticle separation (nearest neighbour) distance (d_s) is given by:

$$d_s = D/\left\{\left(\pi/6V_p\right)^{1/3} - 1\right\} \quad (5)$$

Calculated values of d_s for the composites examined are given in Table 2. Actual values for d_s were also measured (d_{meas}) for some of the materials containing 10% or more of spinel, using a mean line intercept technique on SEM photographs. These values are also given in the table. It is seen that the measured values follow the predicted trends, but are uniformly about 60% too large. This discrepancy is too great to be explained by an arrangement of spinel particles different from the simple cubic array assumed, and the probable reason is that some, perhaps ~6% of the spinel is lost to the system through conversion to the $MgO–Al_2O_3$ solid solution. Values of d_s corrected (d_{corr}) to take into account the loss of spinel in supplying the equilibrium proportion of Al_2O_3 are also shown in the Table. Agreement between measured and calculated values is now very good. Further evidence for the appreciable solid solubility of Al_2O_3 in MgO during hot-pressing has already been seen in the extensive precipitation of fine spinel crystals within the MgO grains in most of the composites formed with larger amounts of spinel. The presence of

Table 2
Spinel particle separation distances, calculated on the assumption of a simple cubic array

	5			10			20			30		
Particle size/μm	d_s/μm	d_{meas}/μm	d_{corr}/μm	d_s/μm	d_{meas}/μm	d_{corr}/μm	d_s/μm	d_{meas}/μm	d_{corr}/μm	d_s/μm	d_{meas}/μm	d_{corr}/μm
3	3.6	–	4.0	2.2	–	4.0	1.1	1.6	1.7	0.6	–	0.9
11	13.1	–	14.5	8.1	–	14.5	4.2	6.0	6.3	2.2	3.8	3.2
22	26.1	–	29.0	16.2	–	29.0	8.3	12.0	10.6	4.5	–	6.4

precipitate-free zones near the MgO grain boundaries confirms that during cooling some of the Al^{3+} ions (from the now supersaturated solution of Al_2O_3 in MgO) are able to escape to the MgO grain boundaries, where for the 5% composites nucleation and growth of fine spinel particles occurs. The tendency for the larger spinel particles also to be located at the MgO grain boundaries is assumed to be the consequence of the extensive MgO grain growth during the later stages of densification, and the enforced migration of spinel particles trapped at slower moving MgO boundaries. The migration of spinel particles locked on to those moving MgO grain boundaries which disappear as a result of the grain growth process is also assumed to account for the clustering (and subsequent partial sintering) of the finer spinel particles. In the composites prepared with larger amounts of spinel, the larger and residual primary spinel surfaces act as nuclei for the recrystallised secondary spinel formed by the Al_2O_3 exsolution; they therefore partially regain their initial volume, with the development of the clean crystal facetting associated with crystal growth, and the grain boundaries are free of fine spinel particles.

Stress generation as a result of thermal expansion mismatch between a matrix and an included particle has been analyzed in detail[41] for the cases of crystalline particles in a glass matrix. The hydrostatic residual stress (S) developed at the surface of a spherical particle of radius R and volume fraction V_p in an isotropic matrix during a temperature change of ΔT is given by:[42]

$$S = \Delta\alpha\Delta T/\{(1-2\nu_s)\}/E_s + [1 + V_p + \nu_m (1-4V_p)]/[2E_m(1-V_p)] \quad (6)$$

where $\Delta\alpha$ is the mean difference in thermal expansion coefficient between MgO and spinel ($\sim$5.9 MK^{-1}), and ν_s and ν_m, and E_s and E_m, are the Poisson ratio and Young's Modulus for spinel and MgO respectively. Assuming an effective cooling temperature of 1100 °C to allow for some high temperature plasticity in the cubic MgO grains, a value for ν of 0.29 for both phases, the measured value for E_m of 268 GPa, and 159 GPa for the spinel 12,13, the tensile stress at the matrix-particle interface is estimated to be in the region of 1.2–1.05 GPa, for the range of spinel additions examined here. The hoop stress ($\sigma_{\theta\theta}$) at a distance r from the centre of a single spherical particle in an infinite matrix (and assumed to represent a satisfactory approximation at low particle concentrations) is given by:[43]

$$\sigma_{\theta\theta} = -0.5S.(r/R)^3 \quad (7)$$

Stress-distance relationships calculated from Eq. (7) are shown in Fig. 12 for particles of the three mean sizes used. The absolute stress at a given distance from the spinel particle is thus larger, the larger the size of the particle. This suggests that there will be a larger tendency for crack propagation to continue once a crack has been initiated at the inclusion surface. Stresses at points corresponding to the mean mid-separation distances ($d_{corr}/2$) for the 22 μm compositions are shown in Fig. 13. For a 22 μm particle the tensile stress is still $\sim$200 MPa at a distance corresponding to the MgO grain dimension. Intergranular cracks would thus be likely to interlink under these conditions, to form a network of sharp intergranular cracks.

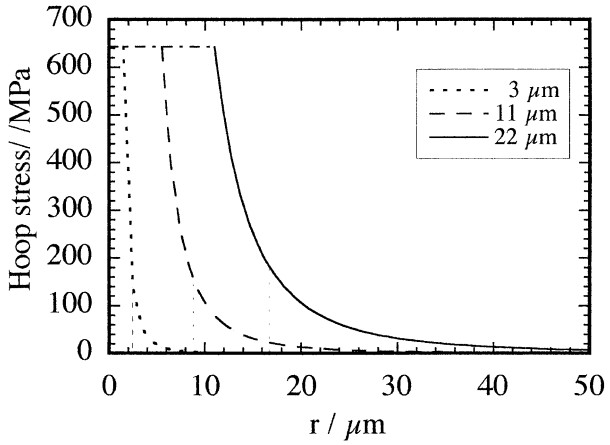

Fig. 12. Stress as a function of distance from particle centre, from Eq. 7.

The consequences of the high temperature solubility of Al_2O_3 (and thus effectively spinel solubility) in MgO require examination. It is clear from the microstructures of the composites that almost 10% of the spinel added dissolves in the MgO during densification at $\sim$1700 °C. Recrystallization of this spinel as fine intragranular and grain boundary, spinel occurs on cooling. Much of this new phase appears to form at spinel particles already at the MgO grain boundaries, and most of the finer spinel particles in the starting powder appear to have been completely redistributed. Growth of the undissolved

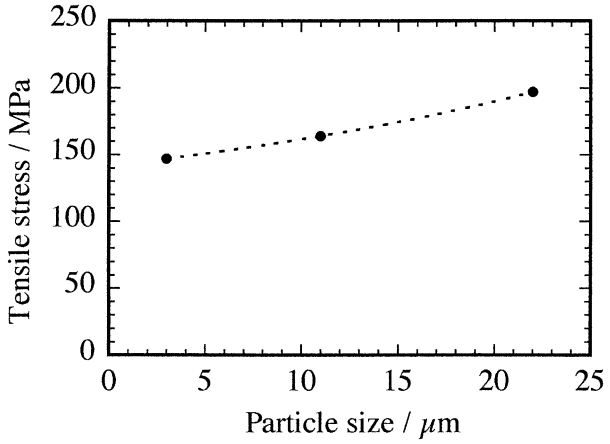

Fig. 13. Stress at (d_{corr})/2 for 20 vol.% spinel, as a function of particle size.

(and larger) spinel particles thus occurs–corresponding to an Ostwald ripening effect.

The mechanism of spinel redistribution is likely to be that of cation diffusion in the oxide lattice. During cooling of the composite, following equilibration at hot-pressing temperature, there is an increase in the chemical potential of Al^{3+}(solution), leading to Al_2O_3 supersaturation in the MgO. As a precursor to the crystallization of spinel, diffusion of Al^{3+} to regions of lower chemical potential occurs; these regions may be low energy sites on the MgO grain boundaries, the surfaces of the undissolved spinel particles, or low energy defect sites such as dislocations within the MgO grains. In order to maintain local electroneutrality, either O^{2-} ions will migrate with the Al^{3+} ions, or simultaneous counter-diffusion of Mg^{2+} ions must occur. Evidence from the mechanism for spinel formation by the solid state reaction of MgO and Al_2O_3[44,45] suggests that, in the confined conditions of a dense material, cation counter diffusion is the dominant process, with the electroneutrality condition:

$$3j_{Al^{3+}} = -2j_{Mg^{2+}} \quad (8)$$

At suitable nuclei, development of spinel crystals into the $MgO_{(solid\ solution)}$ matrix takes place, with outwards displacement of the spinel-solid solution interface into the MgO. This reaction can be written:

$$[MgO - Al_2O_3]_{(solid\ solution)} = MgO_{(c)} + MgAl_2O_{4(c)} \quad (9)$$

Magnesium aluminate is a normal spinel with the oxide ions having the face centred cubic structure. Half of the octahedral sites of the O^{2-} sub-lattice are occupied by Al^{3+}, and one quarter of the tetrahedral sites by Mg^{2+}. The MgO sub-lattices also have the face centred cubic structure. Because the single crystal densities of MgO and spinel are similar, considerable contraction of the O^{2-} lattice must occur when three Mg^{2+} ions in the MgO structure are replaced by two Al^{3+}. Simultaneously, the surrounding MgO lattice, now depleted in Al^{3+}, must expand. The crystallization of spinel particles within the MgO grains and at grain boundaries would thus be expected to generate high local stresses. Relaxation of these stresses will, however, be possible during the higher temperature stages of cooling (>1100 °C) when there is still significant plasticity of the MgO crystal. The magnitudes of these stresses, and the extent to which relaxation on cooling is possible, are hard to gauge, but it might be expected that the actual process of spinel crystallization would not have a very significant residual effect on the stress state of the composite. The dominant stress inducing factor thus seems likely to remain the thermal expansion coefficient differences between the MgO and the spinel. Where the spinel recrystallization process is likely to have a more significant effect is in the location of much of the new secondary spinel, and the growth of remaining primary spinel particles, at the MgO–MgO grain boundaries. The action of the grain boundary spinel particles, and associated thermal expansion mismatch stresses, is illustrated schematically in Fig. 14. Here the tensile hoop stresses around each spinel particle are concentrated at each MgO grain boundary, where they will have maximum weakening effect on the boundary, and may account for the impression that MgO grain boundary separation is occurring. Because the spinel redistribution process reaches a maximum at spinel additions corresponding to the spinel solubility limit in MgO at 1700 to 1725 °C (~6 wt.%), this amount would also represent that for maximizing the potential influence of spinel on grain boundary stress (and thus the effects on mechanical properties of the thermal expansion mismatch). It may therefore not be without significance that the biggest decreases in fracture toughness and thus fracture energy, are seen for the 5 and 10% spinel composites, while the critical defect size remains approximately the MgO grain dimension. The continued fall in strength at higher spinel loadings may be attributable to crack lengthening, by linking and propagation across MgO grains.

With the notable exception of the tetragonal zirconia composites, which because of the possibility of the transformation volume change of the zirconia must be regarded as a special case, similar studies of the influence of particle loading and size in other simple oxide–oxide particulate polycrystalline composites appear not to have been carried out. The nearest approach seems to be that of the Al_2O_3- SiC system, of considerable interest because of the very high toughness, strength, and wear resistance attainable.[46–48] The thermal expansion

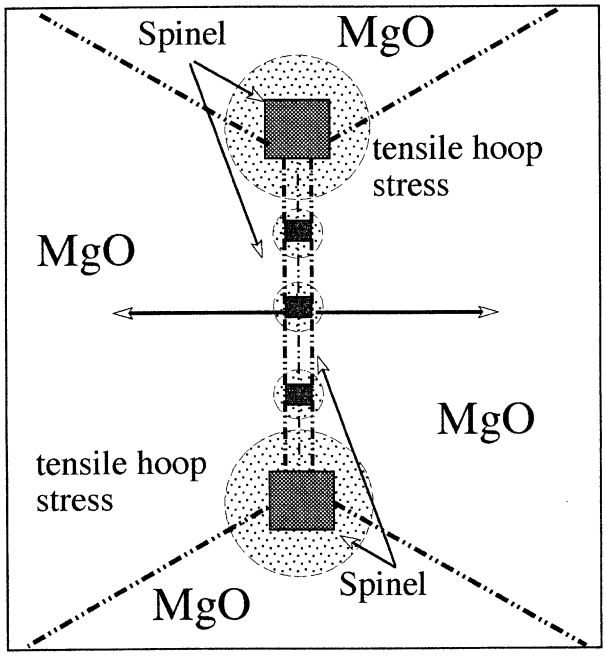

Fig. 14. Schematic diagram showing the influence of spinel particle growth at a grain boundary.

difference between the two phases is very similar, at around 5.5 MK^{-1}, with the inclusion phase also generating tensile stresses in the matrix on cooling. In the Al_2O_3–SiC system, however, fracture toughness increases with addition of SiC up to 24%, and the more so the larger the SiC particles. Strength increases by factors of up to almost 2 at 3% additions, and then decreases: in this case the effect is the more marked the finer the SiC particles.[47] The reasons for the influence of SiC particles in this system are still not established with certainty, but one important feature my be the inclusion particle size. The sizes of spinel used in the present study were considerably larger than most of the silicon carbide particles (which generally tend to the nanosize range). This means that stresses arising from thermal expansion mismatch in the Al_2O_3–SiC composites will diminish very rapidly with distance, and will be very small after a few tens of nanometres from the inclusion surface. For this reason negligible weakening of the alumina-alumina grain boundaries would be expected, in spite of the very large local hoop stresses in the immediate vicinity of the inclusions. If simultaneously grain boundary strengthening occurred, such as is predicted to by the inclusion at the two grain boundaries of thin layers of impurity SiO_2 (almost impossible to avoid with fine silicon carbide powders),[49] then the overall balance would be the creation of a much stronger material. The two systems are different in that no (or very limited) chemical interaction between the SiC particles and the matrix occurs. In the MgO-spinel system in contrast considerable interaction is possible, and this may be the fundamental reason for the differences in mechanical property observed. It is clear, however, that more work on the magnesia-spinel system will be required, and in particular of the use of much finer spinel particles than those in the present study.

5. Conclusions

Microcracking and grain boundary separation, with origins at the MgO–spinel interface occurs in these dense MgO composite materials, as a result of the thermal expansion mismatch between the two phases, and the crystallization of secondary spinel during cooling. These cracks are the critical defects causing failure on loading. The loss of strength and modulus are the greater, the larger the spinel particles, because of the increased extent of the local tensile stress field. Crack interlinking is favoured at high spinel loadings, when inter-spinel particle distances become much smaller than the MgO grain size.

Acknowledgements

Financial support for this work was provided by the Turkish Government. Redland Minerals (UK) and Alcoa International (UK) Ltd. are thanked for supplies of materials. P. Bartha, S. Plint and M.W. Roberts are thanked for helpful discussions. The contributions of the late Professor R.W. Davidge to the planning of this investigation are acknowledged.

References

1. Moore, B., Frith, M. and Evans, D., Developments in basic refractories for cement kilns. *World Cement,* 1991, 5–12.
2. Tabbert, W. and Klischat, H. J., Magnesia spinel bricks for the cement industry. In *Proceedings Beijing China Symposium*, *China*, 1992, pp. 424-30.
3. Kuennecke, M., Wieland K. and Faizullah, M., The correlation between burning zone linings and operation of cement rotary kilns. *World Cement,* 1986, Part 2, 247–253.
4. Bartha, P., Magnesia spinel bricks- properties, production and use. In *Proc. Int. Symp. Refractories, Refractory Raw Materials and High Performance Refractory Products*, ed. X. et al. Zhong. Pergamon, Hangzhou, 1989, pp. 661–674.
5. Reyes Sanchez, J. A. and Toledo, O. D., New developments of magnesite-chrome brick and magnesite-spinel for cement rotary kilns higher thermal shock resistance and higher coating adherence. In *UNITECR 89*, Anaheim, USA, 1989, pp. 968–79.
6. Dal Maschio, R., Fabbri, B. and Fiori, C., Industrial applications of refractories containing magnesium aluminate spinel. *Industrial Ceramics*, 1988, **8**(3), 121–126.
7. Gonsalves, G. E., Duarte, A. K. and Brant, P. O. R. C., Magnesia-spinel brick for cement rotary kilns. *Am. Ceram. Soc. Bull.*, 1993, **72**(2), 49–54.
8. Laurich-McIntyre, S. E. and Bradt, R. C., Room temperature strengths of individual tabular alumina and sintered spinel grains (aggregates). In *UNITECR '93 Congress*, Sao Paulo, Brazil, 1993.
9. Klischat, H. J. and Bartha, P., Further development of magnesia spinel bricks with their own specific properties for lining the transition and sintering zones of rotary cement kilns. *World Cement*, 52–58.
10. Wilson, D. R., Evans, R. M., Wadsworth, I. and Cawley, J., Properties and applications of sintered magnesia alumina spinels. In *UNITECR '93 CONGRESS*, Sao Paulo, Brazil, 1993, pp. 749–60.
11. Kimura, M., Yasuda, Y. and Nishio, H., Development of magnesia spinel bricks for rotary cement kilns in Japan. In *Proc. 26th Int. Col. Ref.*, Interceram Special Issue, 1984, **33**, Aachen, Germany, 1983, 344–76.
12. Shackelford, J. F., Alexander, W., Park, J. S., ed., *CRC Materials Science and Engineering Handbook*. CRC Press, Boca Raton, Florida, 1994.
13. Burnett, S. J., *Properties of Refractory Materials*, UKAEA Research Group Report, Harwell. 1969.
14. Aksel, C., Davidge, R. W., Warren, P. D. and Riley, F. L., Investigation of thermal shock resistance in model magnesia-spinel refractory materials. In *IV. Ceramic Congress*, Proceedings Book, Part 1, Eskisehir, Turkey, 1998, pp. 193–99.
15. Evans, R. M., Magnesia-alumina spinel raw materials production and preparation. *Am. Ceram. Soc. Bull.*, 1993, **72**(4), 59–63.
16. Steetley Magnesia Products Limited, Steetley Co., January 1993, 1–3.
17. Aksel, C., Davidge, R. W., Knott, P. and Riley, F. L., Mechanical properties of magnesia-magnesium aluminate spinel composites. In. *Ceramic Congress Proceedings Book*, Engineering Ceramics, Istanbul, Turkey, 1996, **2**, pp. 172–79.
18. Aksel, C., Davidge, R. W., Warren, P. D. and Riley, F. L., Mechanical properties of model magnesia- spinel composite materials. Euro Ceramics V, Part 3, Extended Abstracts of the

5th Conference and Exhibition of the European Ceramic Society, In *Key Engineering Materials*, Versailles, France, 1997, **132-136**, pp. 1774–77.
19. Hasselman, D. P. H., Elastic energy at fracture and surface energy as design criteria for thermal shock. *J. Am. Ceram. Soc.*, 1963, **46**(11), 535–540.
20. British Standard Testing of Engineering Ceramics, BS 7134 Section 1.2, 1989.
21. Standard Test Methods for flexural strength of advanced ceramics at ambient temperature. In *Annual Book of ASTM Standards*, Designation: C1161-90, **15.01**, 1991, pp. 327–333.
22. Standard Test Methods for flexural properties of unreinforced and reinforced plastics and electrical insulating materials. In *Annual Book of ASTM Standards*, Designation: D790M-86, **08.01**, 1988, pp. 290–298.
23. Larson, D. R., Coppola, J. A., Hasselman, D. P. H. and Bradt, R. C., Fracture toughness and spalling behaviour of high-Al_2O_3 refractories. *J. Am. Ceram. Soc.*, 1974, **57**(10), 417–421.
24. Standard test method for plane-strain fracture toughness of metallic materials. In *Annual Book of ASTM Standards*, Designation: E399-90, **03.01**, 1991, pp. 485–515.
25. Standard Test Methods for plane-strain fracture toughness and strain energy release rate of plastic materials, *Annual Book of ASTM Standards*, Designation: D5045-91, **08.03**, 1991, pp. 728–736.
26. Brown, W. F. and Srawley, J. E., *Plane Strain Crack Toughness Testing of High Strength Metallic Materials*, ASTM Special Technical Publication, No: 410. 1967.
27. Mendelson, M. I., Average grain size in polycrystalline ceramics. *J. Am. Ceram. Soc.*, 1969, **52**(8), 443–446.
28. Davidge, R. W., *Mechanical Behaviour of Ceramics*. Cambridge University Press, Cambridge, 1979.
29. Rice, R. W. Strength and fracture of hot-pressed MgO. Proc. Brit. Ceram. Soc. 1972, (20), 329–63.
30. Itoh, A., Itatani, K., Howell, F. S., Kishioka, A. and Kinoshita, M., Sintering of magnesium oxide powder prepared by vapour-phase oxidation process- Relationship between particle size and mechanical properties of consolidated specimens. *J. Mater. Sci.*, 1996, **31**, 2757–2765.
31. Llorca, J. and Ogawa, T., *Crack Wake Effects on MgO Fracture Resistance, Fracture Mechanics of Ceramics*, eds. Bradt, R. C., Hasselman, D. P. H., Munz, D., Sakai, M. and Shevchenko, V. Ya., 1992, **9**, 305–317.
32. Chiang, Y. M., Birnie D. P. and Kingery, W. D. *Physical Ceramics- Principles for Ceramic Science and Engineering*., New York, 1997.
33. Evans, A. G., Energies for crack propagation in polycrystalline MgO. *Philos. Mag.*, 1970, **22**, 841–852.
34. Davidge, R. W., The texture of special ceramics with particular reference to mechanical properties. In *Proc. Brit. Ceram. Soc.*(20), 364–378.
35. Unchno, J. J., Bradt, R. C. and Hasselman, D. P. H., Fracture surface energies of magnesite refractories. *Am. Ceram. Soc. Bull.*, 1976, **55**(7), 665–668.
36. Stewart, R. L. and Bradt, R. C., Fracture of polycrystalline $MgAl_2O_4$. *J. Am. Ceram. Soc.*, 1980, **63**(11), 619–623.
37. Stewart, R. L. and Bradt, R. C., Fracture of single crystal $MgAl_2O_4$. *J. Mater. Sci.*, 1980, **15**, 67–72.
38. Swanson, G. D., Fracture energies of Ceramics. *J. Am. Ceram. Soc.*, 1972, **55**(1), 48–49.
39. Henriksen, A. F. and Kingery, W. D., The solid solubility of Sc_2O_3, Al_2O_3, Cr_2O_3, SiO_2 and ZrO_2 in MgO. *Ceramurgia Int.*, 1979, **5**(1), 11–17.
40. Hallstedt, B., Thermodynamic assessment of the system MgO-Al_2O_3. *J. Am. Ceram. Soc.*, 1992, **75**(6), 1497–1507.
41. Davidge, R. W. and Green, T. J., The strength of two-phase ceramic/glass materials. *J. Mater. Sci.*, 1968, **3**, 629–634.
42. Wang, X. L., Becher, P. F., Alexander, K. B., Fernandez-Baca, J. A. and Hubbard, C. R., Residual stresses in Al_2O_3-ZrO_2 ceramic composites. In *Proceedings of the 4th International Conference on Residual Stresses*, Society for Experimental Mechanics, Bethel CT, Baltimore MD, 1994, pp. 1172–1177.
43. Selsing, J., Internal stresses in ceramics. *J. Am. Ceram. Soc.*, 1961, **44**(8), 419.
44. Carter, R. E., Mechanism of solid-state reaction between magnesium oxide and aluminium oxide and between magnesium oxide and ferric oxide. *J. Am. Ceram. Soc.*, 1961, **44**(3), 116–120.
45. Beretka, J. and Brown, T., Effect of particle size on the kinetics of the reaction between magnesium and aluminium oxides. *J. Am. Ceram. Soc.*, 1983, **66**(5), 383–388.
46. Zhao, J., Stearns, L. C., Harmer, M. P., Chan, H. M., Miller, G. A. and Cook, R. F., Mechanical behavior of alumina-silicon carbide nanocomposites. *J. Am. Ceram. Soc.*, 1993, **76**(2), 503–510.
47. Ohiji, T., Hirano, T., Nakahira, A. and Niihara, K., Particle/matrix interface and its role in creep inhibition in alumina/silicon carbide nanocomposites. *J. Am. Ceram. Soc.*, 1996, **79**(1), 33–45.
48. Zhang, D., Yang, H., Yu, R. and Weng, W., Mechanical properties of Al_2O_3-SiC composites containing various sizes and fractions of fine SiC particles. *J. Mater. Sci. Lett.*, 1997, **16**(11), 877–879.
49. Blonski, S. and Garofalini, S. H., Atomistic structure of calcium silicate intergranular films in alumina studied by molecular dynamics simulation. *J. Am. Ceram. Soc.*, 1997, **80**(8), 1997–2004.